CO_2 exchange coefficients from remotely sensed wind speed measurements: SSM/I versus QuikSCAT in 2000

Mary-Elena Carr, Wenqing Tang, W. Timothy Liu

Jet Propulsion Laboratory, California Institute of Technology, MS 300-323, 4800 Oak Grove Dr., Pasadena, CA 91009

Abstract.
We compare here the air-sea exchange coefficient for CO_2 estimated with monthly mean wind speed measured by the Special Sensing Microwave Imager (SSM/I), K_S, and by the scatterometer QuikSCAT, K_Q, for the year 2000. K_S and K_Q present the same patterns, although K_S are larger than K_Q in ~65% of the world ocean. Zonal mean K_S are consistently larger, except ~50°S and north of 10°S in the Indian Ocean. Global oceanic uptake, F_Q, estimated using K_Q and climatological Δp_{CO_2} ranges from 0.43 (July) to 2.6 Gt C y^{-1} (December). The global sink estimated from SSM/I is ~10% larger than F_Q for most of the year. This comparison supports the use of SSM/I to quantify interannual variability of the global exchange coefficient of CO_2 .

1. Introduction

Approximately half of annual anthropogenic CO_2 emissions is taken up by the terrestrial biosphere and by the ocean (Feely *et al.*, 2002). The growth of the atmospheric concentration of CO_2 varies considerably from year to year despite relatively invariant emission rates (Keeling *et al.*, 1995). Atmospheric inversion models ascribe this variability to changes in oceanic uptake of 1-3 Gt C y^{-1} (Battle *et al.*, 2000). However, interannual variability in the air-sea flux, estimated from extrapolations of measured oceanic CO_2 concentrations based on its relationship with sea surface temperature (SST) (Lee *et al.*, 1998) and from ocean circulation models with simple biogeochemistry (Lequéré *et al.*, 2000), is at most 0.4 Gt C. In these studies, the air-sea exchange coefficient (K) accounts for less than 20-30% of the interannual variability. We believe that climatological or modeled wind speeds likely underestimate variability in the exchange coefficient. Our ultimate goal is to use the existing 13-year time series of wind speed measurements from the Special Sensing Microwave Imager (SSM/I) to quantify interannual variability in K for this period. The uncertainty in wind speed derived from SSM/I (1-3 ms^{-1}) is greater than that of the scatterometer QuikSCAT (~ 1 ms^{-1}), flying since late 1999 (Wentz,

1997; Liu, 2002). Because of this smaller uncertainty and the ability to measure wind direction, although we do not use it here, we consider QuikSCAT our 'best quality' wind speed source. In this study we compare the exchange coefficient estimated from SSM/I, K_S, with that estimated from QuickSCAT, K_Q, to evaluate the results obtained from SSM/I.

2. Background

The flux of CO_2 between ocean and atmosphere is given by $F = K * \Delta p_{CO_2}$ where Δ pCO_2 is the difference in partial pressure between the ocean and the atmosphere. The exchange coefficient, is given by $K = s * k_{ave}$ where s is the solubility of CO_2 and k_{ave} is the long-term gas transfer velocity (Wanninkhof, 1992), which depends on turbulence in the water boundary layer. There exist a range of parameterizations for the gas transfer velocity as a function of wind speed (Nightingale *et al.*, 2000, and references therein) which vary by a factor of two or more globally (*e.g.*, Feely *et al.*, 2002; Boutin *et al.*, 2002). Wind-based parameterizations only provide an indirect estimate of K because they neglect, for example, explicit consideration of bubbles and surfactants, but they represent the easiest available approach, especially on the global scale.

Three months of measurements from the Seasat scatterometer in 1978 provided a global estimate of K that was consistent with previous values (Etcheto and Merlivat, 1988). Boutin and Etcheto (1991) concluded that the error in K due to the spatial integration and temporal sampling inherent to satellite wind measurements was less than the uncertainty associated with the choice of wind speed parameterization. Variability of K, estimated from the Geosat altimeter and SSM/I (1985-1992), was much larger at seasonal time scales than from year to year at high northern latitudes, while interannual variability in the tropics and in the Southern Ocean could match or exceed seasonal changes (Boutin and Etcheto, 1997). The accuracy of K in the equatorial Pacific derived from SSM/I was order $0.14 \cdot 10^{-2}$mol $m^{-2}y^{-1}\mu atm^{-1}$, an 8% relative error, while the scatterometer errors (ERS1/2 and NSCAT) were smaller (Boutin *et al.*, 1999a). NSCAT-based K estimates were in excellent agreement with those from wind speeds made by the CARIOCA drifter for the month of January 1997 in the equatorial Pacific, while SSM/I overestimated the wind speed (Boutin *et al.*, 1999b).

3. Data and Methods

We derived K using the formulation given above, where k_{ave} was estimated from the long-term average wind (monthly mean for 2000) and the Schmidt number. We correct for the dependence on temperature (Schmidt number and solubility) and on salinity (solubility) as in Wanninkhof (1992). The wind speeds are monthly averages of the wind speed produced within NASA's Pathfinder Program (http://www.SSMI.com/ssmi/) for SSM/I and those of Tang and Liu (http://airsea-www.jpl.nasa.gov /seaflux/) for QuikSCAT. The monthly mean temperature fields for 2000 are an optimally interpolated combination of Advanced Very High Resolution Radiometer (AVHRR) and ship observations (Reynolds and Smith, 1994). We used climatological salinity fields from the World Ocean Atlas 1998 (http://www.nodc.noaa.gov). The air-sea flux of CO_2 was estimated using the monthly mean K for 2000 and climatological maps of Δ pCO_2 (http://ingrid.ldgo.columbia.edu /SOURCES/.LDEO/.Takahashi/; Takahashi *et al.*, 1997) which refer to 1995.

4. Results

K estimated from the two sensors present the same patterns, though K_S exceeds K_Q in ~65% of the world ocean. The annual mean (non-area-weighted) K_S and K_Q are 7.41 and 7.07 $\cdot 10^{-2}$mol $m^{-2}y^{-1}\mu atm^{-1}$ respectively. The global monthly mean K_S surpasses K_Q by 0.16 (2%) to 0.6$\cdot 10^{-2}$mol $m^{-2}y^{-1}\mu atm^{-1}$ (6.5%).

The non-area-weighted zonal mean values (Figure 1a) follow the pattern described by Boutin and Etcheto (1997) with maxima associated with the westerlies (~50° : 8-10 $\cdot 10^{-2}$mol $m^{-2}y^{-1}\mu atm^{-1}$) and the trade winds (~15° : 5-8 $\cdot 10^{-2}$mol $m^{-2}y^{-1}\mu atm^{-1}$) and minima (<4 $\cdot 10^{-2}$mol $m^{-2}y^{-1}\mu atm^{-1}$) within 10° of the equator. The global mean ΔK (K_S-K_Q) is consistently positive except at 50°S (Figure 1b) and is minimum within 5° of 0°. ΔK in the Indian Ocean exceeds 1 $\cdot 10^{-2}$mol $m^{-2}y^{-1}\mu atm^{-1}$ at 20-25°S and is <-1 $\cdot 10^{-2}$mol $m^{-2}y^{-1}\mu atm^{-1}$ north of 15°N. These K_S are consistent with those of Boutin and Etcheto (1997) in spite of different data handling, product version, and study period. The major discrepancy, the higher equatorial values seen here, are likely due to the new Pathfinder algorithm, as Boutin *et al.* (1999b) found that SSM/I overestimated winds in the equatorial Pacific.

The seasonal cycle of K in the Atlantic and Pacific is weak in the equatorial band (10°N-10°S) and maximum poleward of 40° ; peak amplitude is 8-10 $\cdot 10^{-2}$mol

$m^{-2}y^{-1}\mu atm^{-1}$ north of 40°N in the Atlantic (Figure 2a). The equatorial (10°S-10°N) and tropical (>10°N) regions of the Indian Ocean reflect the monsoonal forcing. K is maximum in hemispheric winter in the Atlantic and Pacific and southern Indian Oceans (winter storms). The largest ΔK in the Atlantic and Pacific are $\sim 1 \cdot 10^{-2}$mol $m^{-2}y^{-1}\mu atm^{-1}$ and occur in hemispheric fall and winter poleward of 10°. In the Indian Ocean, ΔK is consistently negative between 10°S and 25°N. SSM/I underestimates wind speed in the Arabian Sea in the monsoon period (*e.g.* Meissner *et al.*, 2001), likely due to the geometry of sensor viewing and wind direction, and to the presence of cold upwelled water. Discrepancies at high latitudes in winter may be related to the tendency of SSM/I to overestimate high wind speeds or to precipitation (which also affects QuikSCAT). Though ΔK is largest at high wind speeds due to the quadratic expression for K, we found no systematic relationship between ΔK and wind speed. ΔK obviously depends on both sensors, neither of which is perfect. However, our assumption that QuikSCAT is the best quality wind product is supported by the similarity of the ΔK distribution with other studies (Meissner *et al.*, 2001).

The global mean flux is always into the ocean; it is lowest in July and peaks in December. Flux from QuikSCAT, F_Q, is -0.43 to -2.56 Gt C y^{-1}, and that from SSM/I, F_S, between -0.61 and -2.76 Gt C y^{-1}. The consistently larger K_S values translate into ΔF from -0.02 to -0.25 Gt C y^{-1} (Figure 3a). F_S is at most 11% larger than F_Q, except in July and August (F_S is 40-50% larger) when flux is minimum. The Atlantic and Indian Oceans are basin averaged sinks throughout 2000 (Figure 3b), while the Pacific is a weak source (< 0.4 Gt C y^{-1}) in boreal summer (June through September). The Atlantic basin is the strongest sink: F_S and F_Q are <-0.8 Gt C y^{-1} from October to April. Mean flux into the Indian Ocean is < -0.5 Gt C y^{-1} between April and December. F_S on the basin average is consistently a larger sink than F_Q in the Atlantic and Indian Oceans, while it is weaker than or close to F_Q most of the year in the Pacific (Figure 3b).

The seasonal cycle of flux is most pronounced between 10°N and 40°N (all basins) and between 10°S and 40°S in the Indian Ocean (Figure 4a). Major sinks ($\sim$ -0.5 Gt C y^{-1}) are found year-round south of 40°S (all basins) and poleward of 40°N in the Atlantic. The equatorial band (10°S-10°N) is a source year-round: $\sim$0.1 Gt C y^{-1} in the Atlantic and Indian and >0.5 Gt C y^{-1} in the Pacific. The Indian Ocean is a strong sink between 10°S and 40°S (<-0.5 Gt C y^{-1} between June

and November) and a year-round source north of 10°N, peaking June through September (~0.35 Gt C y^{-1}). Our basin estimates (including the southern ocean) of F_Q (F_S) of -0.69 (-0.74), -0.20 (-0.19), -0.58 (-0.68) Gt C y^{-1} for the Atlantic, Pacific, and Indian respectively are in reasonable agreement with those of Feely *et al.* (2002): (north of 50°S) of -0.69, -0.21, -0.33 Gt C y^{-1}, plus -0.58 Gt C y^{-1} for the Southern Ocean.

ΔF exceeds 0.05 Gt C y^{-1} in the equatorial Pacific, between 10°N and 40°N in the Pacific and Indian, and between 10°S and 40°S in the Indian Ocean (Figure 4b). In the Atlantic, ΔF is always within ±0.05 Gt C y^{-1} . The ΔK distribution in the Atlantic and Pacific basins is comparable in both source and sink regions, so flux compensates in the basin mean. By contrast in the Indian Ocean, ΔK is negative (north of 10°S) in regions of positive Δ pCO_2 and positive in the region of negative Δ pCO_2 (10-40°S). The net result is that uptake estimated by SSM/I is consistently larger than that estimated from QuikSCAT north of 40°S.

5. Conclusions

The product versions of the two sensors used in this study provide comparable estimates of K and flux. Future changes in the products will likely further decrease the discrepancies (Wentz, pers. comm.). Although K_S is larger than K_Q in the comparison year 2000, the flux estimate in the Atlantic and Pacific is compensated. In the Indian Ocean, ΔK changes sign with Δ pCO_2 , leading to a greater mismatch of flux estimates. Globally, the discrepancies in K of ~0.3 $\cdot 10^{-2}$mol $m^{-2}y^{-1}\mu atm^{-1}$ (5%) translate to uncertainties in flux on the order of 0.12 Gt C (9%). These results validate the use of SSM/I to study interannual variability in the global exchange coefficient of CO_2 . Ongoing comparison of K_Q and K_S will improve our understanding of the regional differences and enable quantitative use of K_S for periods in which we do not have scatterometer data.

Acknowledgements

We thank Frank Wentz for the SSM/I data and several valuable suggestions and Taro Takahashi for the climatological Δ pCO_2 fields. Richard Feely and Rik Wanninkhof provided helpful discussions and comments on an earlier version. We are grateful to Xiaosu Xie for providing monthly mean QuikSCAT wind speed data from PODAAC to compare with the Tang and Liu product and to two anonymous reviewers for thorough comments that improved the original manuscript. The re-

search described in this paper was carried out at the Jet Propulsion Laboratory, California Institute of Technology, under a contract with the National Aeronautics and Space Administration.

References

Battle, M., Bender, M. L., Tans, P., White, J., Ellis, J., Conway, T., and Francey, R. Global carbon sinks and their variability inferred from atmospheric O_2 and δC_{13}. *Science, 287* (5462): 2467–2470. 2000.

Boutin, J. and Etcheto, J. Intrinsic error in the air-sea CO_2 exchange coefficient resulting from the use of satellite wind speeds. *Tellus-B, 43 (2)*: 236–246. 1991.

Boutin, J. and Etcheto, J. Long-term variability of the air-sea CO_2 exchange coefficient: Consequences for the CO_2 fluxes in the equatorial Pacific Ocean. *Global Biogeochemical Cycles, 11 (3)*: 453–470. 1997.

Boutin, J., Etcheto, J., Dandonneau, Y., Bakker, D., Feely, R. A., Inoue, H. Y., Ishii, M., Ling, R., Nightingale, P., Metzl, N., and Wanninkhof, R. Satellite sea surface temperature: a powerful tool for interpreting in situ pCO_2 flux measurements in the equatorial Pacific Ocean. *Tellus-B, 51(2)*: 490–508. 1999a.

Boutin, J., Etcheto, J., Merlivat, L., and Rangama, Y.. Influence of gas exchange coefficient parameterisation on seasonal and regional variability of CO_2 air-sea fluxes. *Geophysical Research Letters 29 (8)*, 2002.

Boutin, J., Etcheto, J., Rafizadeh, M., and Bakker, D. Comparison of NSCAT, ERS2 Active Microwave Instrument, Special Sensor Microwave Imager, and CARbon Interface Ocean Atmosphere buoy wind speed: Consequences for the air-sea CO_2 exchange coefficient. *Journal of Geophysical Research, 104*: 11375–11392. 1999b.

Etcheto, J. and Merlivat, L. Seasonal variation of the CO_2 air-sea exchange coefficient over the gloval ocean using satellite wind-speed measurements. *Tellus-B, 43 (2)*: 247–255. 1988.

Feely, R. A., Sabine, C., Takahashi, T. and Wanninkhof, R. Uptake and storage of carbon dioxide in the ocean: the global CO_2 survey. *Oceanography, 14 (4)*: 18–32. 2002.

Keeling, C. D., Whorf, T. P., Wahlen, M., and Vanderplicht, J. Interannual extremes in the rate of rise of atmospheric carbon dioxide since 1980. *Nature, 375 (6533)*: 666–670. 1995.

Le Quéré, C., Orr, J., Monfray, P., Aumont, O., and Madec, G. Interannual variability of the oceanic sink of CO_2 from 1979 through 1997. *Global Biogeochemical Cycles, 14 (4)*: 1247–1265. 2000.

Lee, K., Wanninkhof, R., Takahashi, T., Doney, S. C., and Feely, R. A. Low interannual variability in recent oceanic uptake of atmospheric carbon dioxide. *Nature, 396 (6707)*: 155–159. 1998.

Liu, W. T. 2002 Progress in scatterometer application. *Journal of Oceanography, 58*: 121–136. 2002.

Meissner, T., D. Smith, and Wentz, F. A 10-year intercomparison between collocated Special Sensor Microwave Imager oceanic surface wind speed retrievals and global analyses. *Journal of Geophysical Research, 106*: 11,731–11,742. 2001.

Nightingale, P. D., Malin, G., Law, C. S., Watson, A. J., Liss, P. S., Liddicoat, M. I., Boutin, J., and Upstill-Goddard, R. In situ evaluation of air-sea gas exchange parameterizations using novel conservative and volatile tracers. *Global Biogeochemical Cycles, 14 (1)*: 373–387. 2000.

Reynolds, R. W. and Smith, T. Improved sea surface temperature analysis using optimum interpolation. *Journal of Climate, 7*: 929–948. 1994.

Takahashi, T., Feely, R., Weiss, R., Wanninkhof, R., Chipman, D., Sutherland, S., and Takahashi, T. T. Global air-sea flux of CO_2: An estimate based on measurements of sea-air pCO_2 difference. *Proc. National Academy of Sciences U. S. A., 94 (16)*: 8292–8299. 1997.

Wanninkhof, R. Relationship between wind-speed and gas-exchange over the ocean. *Journal of Geophysical Research, 97*: 7373–7382. 1992.

Wentz, F. A well calibrated ocean algorithm for SSM/I. *Journal of Geophysical Research, 102*: 8703–8718. 1997.

M. -E. Carr, Jet Propulsion Laboratory, California Institute of Technology, M/S 300-323, 4800 Oak Grove Dr, Pasadena CA 91109-8099, mec@pacific.jpl.nasa.gov

(Received _____)

Figure 1. Zonal mean of the annual average K_Q for the globe and for each basin (a) and the difference between K_S and K_Q for the globe and each basin (b). Figure (a) is not area-weighted; high latitudes represent small oceanic area.

Figure 1. Zonal mean of the annual average K_Q for the globe and for each basin (a) and the difference between K_S and K_Q for the globe and each basin (b). Figure (a) is not area-weighted; high latitudes represent small oceanic area.

Figure 2. Seasonal progression of mean K_Q and K_S within latitude bands in each basin for 2000 (a). The solid (dashed) lines are the mean K_Q (K_S). Seasonal progression of ΔK (b). Figure (a) is not area-weighted; high latitudes represent small oceanic area.

Figure 2. Seasonal progression of mean K_Q and K_S within latitude bands in each basin for 2000 (a). The solid (dashed) lines are the mean K_Q (K_S). Seasonal progression of ΔK (b). Figure (a) is not area-weighted; high latitudes represent small oceanic area.

Figure 3. Monthly global average of CO_2 flux (a), and for each basin (b) for 2000. The solid (dashed) lines are the mean F_Q (F_S) in (b).

Figure 3. Monthly global average of CO_2 flux (a), and for each basin (b) for 2000. The solid (dashed) lines are the mean F_Q (F_S) in (b).

Figure 4. Monthly global average of CO_2 flux for each basin for 2000 (a). The solid (dashed) lines are the mean F_Q (F_S) in the upper. Seasonal progression of ΔF (b).

Figure 4. Monthly global average of CO_2 flux for each basin for 2000 (a). The solid (dashed) lines are the mean F_Q (F_S) in the upper. Seasonal progression of ΔF (b).

CARR ET AL.: SSM/I AND QUIKSCAT AIR-SEA CO2 EXCHANGE

CARR ET AL.: SSM/I AND QUIKSCAT AIR-SEA CO2 EXCHANGE

CARR ET AL.: SSM/I AND QUIKSCAT AIR-SEA CO2 EXCHANGE

CARR ET AL.: SSM/I AND QUIKSCAT AIR-SEA CO2 EXCHANGE

CARR ET AL.: SSM/I AND QUIKSCAT AIR-SEA CO2 EXCHANGE

CARR ET AL.: SSM/I AND QUIKSCAT AIR-SEA CO2 EXCHANGE

CARR ET AL.: SSM/I AND QUIKSCAT AIR-SEA CO2 EXCHANGE

CARR ET AL.: SSM/I AND QUIKSCAT AIR-SEA CO2 EXCHANGE

CARR ET AL.: SSM/I AND QUIKSCAT AIR-SEA CO2 EXCHANGE

CARR ET AL.: SSM/I AND QUIKSCAT AIR-SEA CO2 EXCHANGE

CARR ET AL.: SSM/I AND QUIKSCAT AIR-SEA CO2 EXCHANGE

CARR ET AL.: SSM/I AND QUIKSCAT AIR-SEA CO2 EXCHANGE

CARR ET AL.: SSM/I AND QUIKSCAT AIR-SEA CO2 EXCHANGE

CARR ET AL.: SSM/I AND QUIKSCAT AIR-SEA CO2 EXCHANGE

CARR ET AL.: SSM/I AND QUIKSCAT AIR-SEA CO2 EXCHANGE

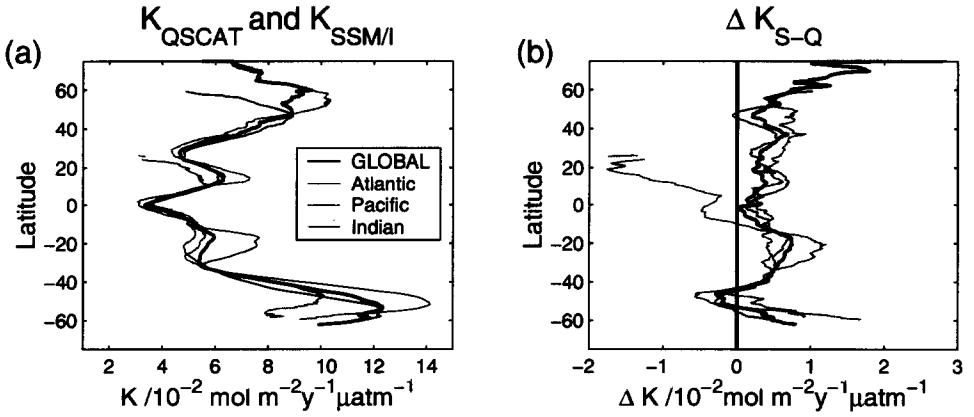

FIG. 1. Zonal mean of the annual average K_Q for the globe and for each basin (a) and the difference between K_S and K_Q for the globe and each basin (b). Figure (a) is not area-weighted; high latitudes represent small oceanic area.

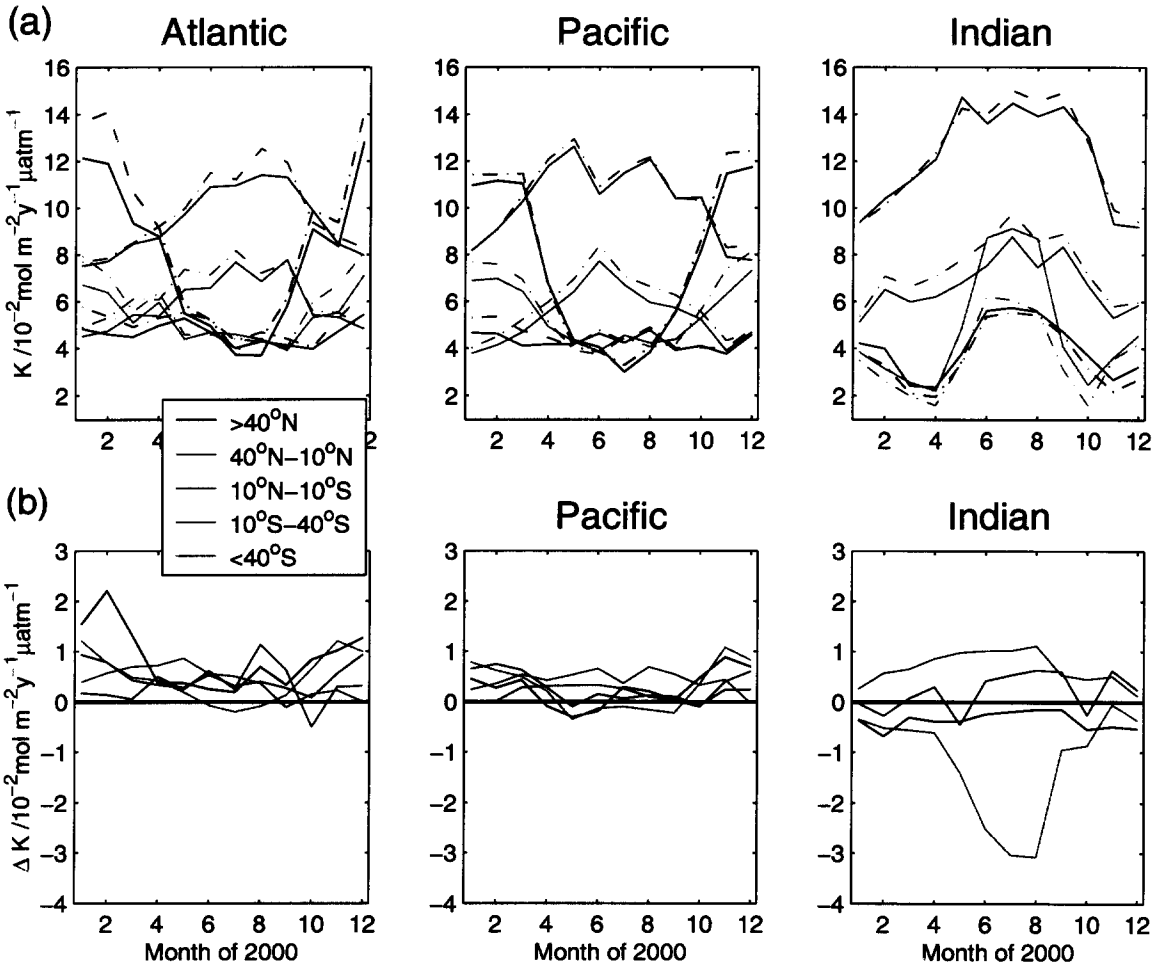

FIG. 2. Seasonal progression of mean K_Q and K_S within latitude bands in each basin for 2000 (a). The solid (dashed) lines are the mean K_Q (K_S). Seasonal progression of ΔK (b). Figure (a) is not area-weighted; high latitudes represent small oceanic area.

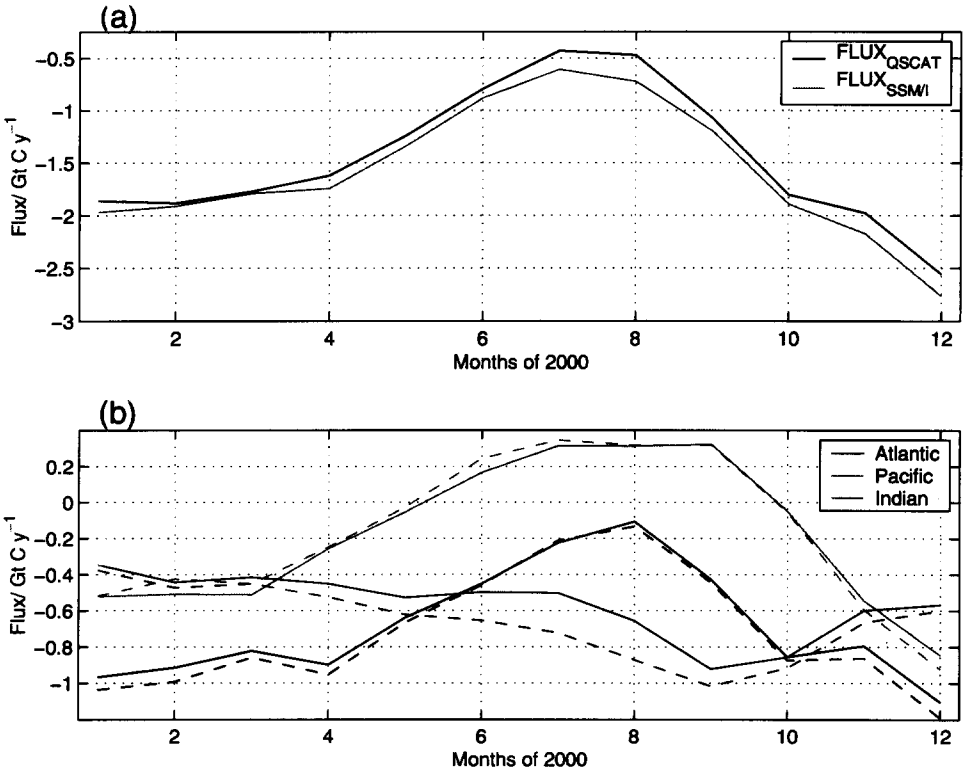

FIG. 3. Monthly global average of CO_2 flux (a), and for each basin (b) for 2000. The solid (dashed) lines are the mean F_Q (F_S) in (b).

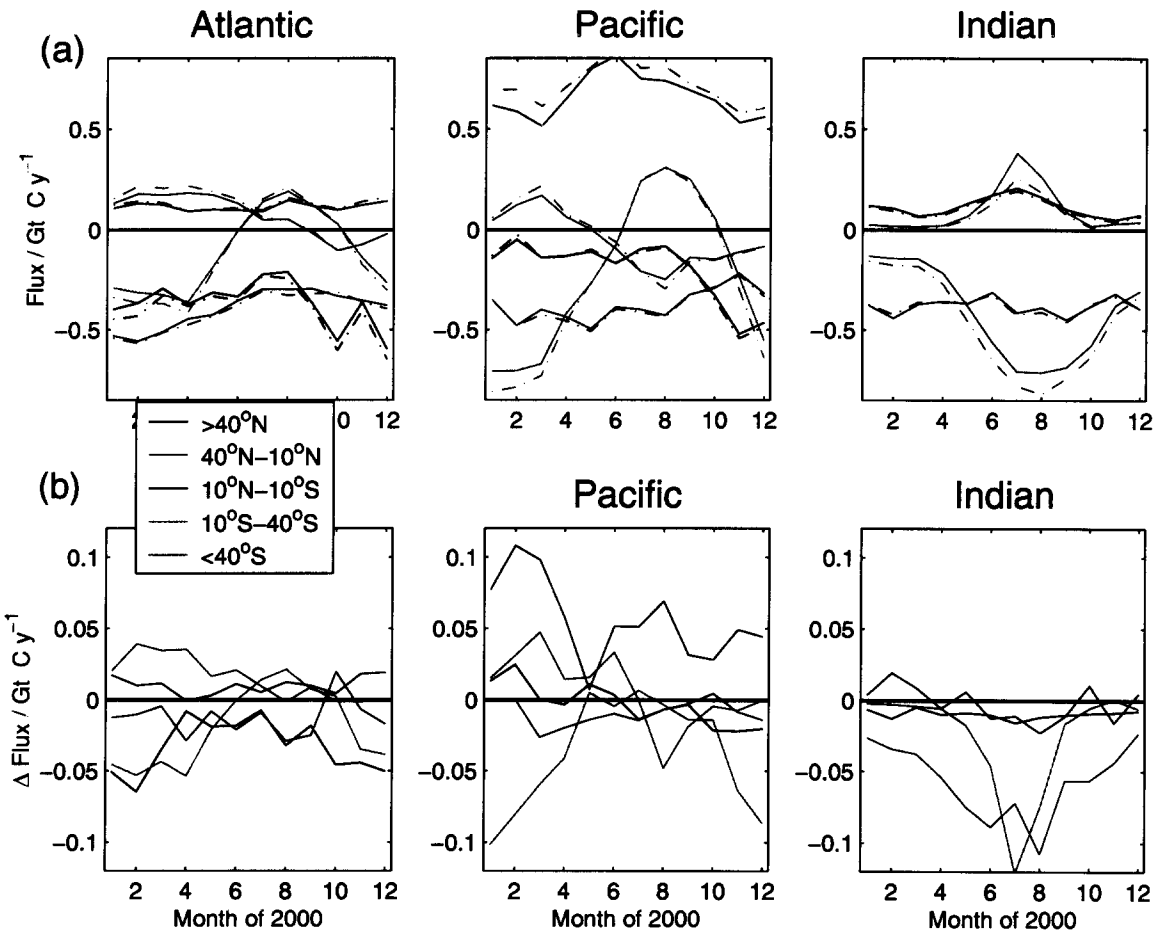

FIG. 4. Monthly global average of CO_2 flux for each basin for 2000 (a). The solid (dashed) lines are the mean F_Q (F_S) in the upper. Seasonal progression of ΔF (b).